Chinese Chemical Letters 33 (2022) 5035–5041

Contents lists available at ScienceDirect

Chinese Chemical Letters

journal homepage: www.elsevier.com/locate/cclet

Folate-targeted co-delivery polymersomes for efficient photo-chemo-antiangiogenic therapy against breast cancer and *in vivo* evaluation *via* OCTA/NIRF dual-modal imaging

Hongjun Wu[1], Chenlu Huang[1], Liwei Wang, Qinghua Li, Yuejie Li*, Linhua Zhang*, Dunwan Zhu*

Tianjin Key Laboratory of Biomedical Materials, Key Laboratory of Biomaterials and Nanotechnology for Cancer Immunotherapy, Institute of Biomedical Engineering, Chinese Academy of Medical Sciences & Peking Union Medical College, Tianjin 300192, China

ARTICLE INFO

Article history:
Received 7 March 2022
Revised 7 April 2022
Accepted 7 April 2022

Keywords:
Polymersomes
Optical coherence tomography angiography (OCTA)
Near infrared fluorescence (NIRF) imaging
Photo-chemo-antiangiogenic therapy
Intelligent nanoplatform

ABSTRACT

Intelligent nanoplatform that combines multimodal imaging and therapeutic effects holds great promise for precise and efficient cancer therapy. Herein, folate-targeted polymersomes with stimuli-responsiveness were fabricated and evaluated by near-infrared fluorescence (NIRF) and optical coherence tomography angiography (OCTA) dual-imaging for photo-chemo-antiangiogenic therapy against cancer. The folate-targeted polymersomes (FA-MIT-SIPS) not only integrated ammonium bicarbonate (ABC) and mitoxantrone (MIT) into their hydrophilic cavity but also encapsulated indocyanine green (ICG) and sorafenib (SOR) within their hydrophobic layer. NIRF imaging demonstrated that FA-MIT-SIPS effectively accumulated and retained in the tumors. Upon 808 nm laser irradiation, the ICG produced hyperthermia and reactive oxygen species (ROS) for efficient photothermal and photodynamic therapy. In addition, the decomposition of ABC in responsive to acidic tumor environment and ICG-induced hyperthermia accelerated drug release. The released MIT accumulated in nucleus to inhibit DNA synthesis, while the released SOR destructed tumor vascularization. Notably, OCTA imaging was applied to observe the tumor blood flow upon the combination therapy, demonstrating that FA-MIT-SIPS obviously decreased the vessels area density. Moreover, the synergistic photo-chemo-antiangiogenic therapy of FA-MIT-SIPS achieved excellent antitumor effect with 40% of the 4T1 tumor-bearing mice being completely cured without recurrence. The multifunctional polymersomes provide a promising dual-modal imaging-evaluated synergistic strategy for tumor therapy.

Cancer is severely threatening human life and health because of high morbidity and mortality [1]. As a main cancer treatment approach in clinic, chemotherapy is able to directly eradicate cancer cells and has gained prominent success in prolonging patient survival. Nevertheless, chemotherapeutic drugs are subject to rapid clearance, nonspecific distribution, and serious side effects [2]. Meanwhile, multi-drug resistance (MDR) of cancer cells severely hinders the chemotherapeutic effectiveness [3]. Phototherapy, including photothermal therapy (PTT) and photodynamic therapy (PDT), has been developed as a safe and efficient approach for cancer treatment in recent years [4]. Under laser irradiation, PTT utilizes photothermal conversion agents to produce hyperthermia for the eradication of cancer cells, while PDT involves the use of photosensitizer to generate ROS to cause cell death [5]. However, as a local precision therapy, phototherapy cannot completely eliminate cancer in the whole body. To improve cancer therapeutic effect, the integration of phototherapy and chemotherapy has been widely studied and showed remarkable synergistic effects [6]. The hyperthermia induced by PTT can not only directly kill cancer cells, but also promote cellular uptake and intracellular release of chemotherapeutic drugs to improve their cytotoxicity [7]. Meanwhile, the ROS generated by PDT can facilitate intracellular drug delivery and release to increase cytotoxicity [8]. Despite the encouraging effect of phototherapy-enhanced chemotherapy, the anticancer efficacy remains limited and needs to be further improved because of the complexity and diversity of tumor microenvironment [9].

* Corresponding authors.
E-mail addresses: liyj@bme.pumc.edu.cn (Y. Li), zhanglinhua@bme.pumc.edu.cn (L. Zhang), zhudunwan@bme.pumc.edu.cn (D. Zhu).
[1] These authors contributed equally to this work.

https://doi.org/10.1016/j.cclet.2022.04.021
1001-8417/

Tumor tissue is surrounded by a network of blood vessels, which provide nutrition for rapid tumor growth [10]. Therefore, antiangiogenic therapy aimed to destroy tumor vascularization has become a promising strategy in cancer treatment [11]. Up to now, many antiangiogenic agents have been discovered to decrease the production of proangiogenic factors and halt angiogenic process, leading to the suppression of tumor growth and metastasis [12]. Sorafenib (SOR), a multi-kinase inhibitor that can restrain vascular endothelial growth factor (VEGF) and platelet-derived growth factor (PDGF) receptors to block angiogenesis, is approved by FDA to treat metastatic renal cell carcinoma [13]. Besides, SOR is capable of suppressing cell proliferation and inducing cell apoptosis [14]. Recently, the combination therapy of SOR with chemotherapeutic drug doxorubicin (DOX) considerably improved the overall survival rate of patients in clinical trial studies [15,16]. Nevertheless, the poor water solubility, rapid drug metabolism, and low bioavailability of SOR severely hindered the combinational therapeutic effect [17]. With the rapid development of nanotechnology, numerous nano-formulations have been designed to overcome the above disadvantages and enhance combination antitumor effect [18,19]. For example, Sui *et al.* [15] formulated pH-sensitive nanoparticles to co-deliver SOR and DOX (P-Dox NPs). Their studies demonstrated that P-Dox NPs facilitated drug accumulation in tumor site and achieved obviously better synergistic antitumor effect with reduced side effects against breast carcinoma than free drugs.

For accurate and efficient cancer treatment, intelligent nanoplatforms that combine multimodal imaging and therapeutic agents have attracted increasing attention [20]. Among various nanoplatforms, polymersomes based on amphiphilic copolymers have unique structures to efficiently encapsulate both hydrophobic and hydrophilic agents within their membrane and lumen respectively [21]. In addition, polymersomes have the merits of good colloidal stability and easy surface ligand modification, enabling them to deliver drugs into tumor site without premature leakage during blood circulation and reduce severe side effect *via* tumor targeting ability [22]. Furthermore, intelligent polymersomes can be designed to induce site-specific release of loaded therapeutics in responsive to intrinsic stimuli (*e.g.*, pH, redox, enzyme, temperature) and/or extrinsic stimuli (*e.g.*, light, ultrasound, magnetic field) [5,8,23]. To continuously monitor the therapeutic efficacy and provide personalized medicine, imaging-guided drug delivery nanoplatforms have been designed for precision cancer diagnosis and therapy [24]. As a non-invasive imaging tool with high sensitivity and rapid imaging speed, near-infrared fluorescence (NIRF) imaging has been extensively developed as a promising approach for cancer diagnosis and therapeutic monitoring as well as pharmacokinetic observation of drugs in pre-clinical research [25]. Nevertheless, NIRF imaging exhibits limited spatial resolution and is unable to evaluate tumor vascularization, which is an important indicator for tumor antiangiogenic therapy.

With the development of optical technologies, the change of microvascular functional information can be effectively imaged before and after treatment by the optical coherence tomography angiography (OCTA) technology [26]. Coherent light could be reflected or scattered by different levels of tissue. The anatomic information of the sample is obtained by the interference signal. The reconstruction of tumor blood vessels is realized according to the algorithm [27–29]. Compared with other imaging technologies, OCT can achieve high-resolution, fast real-time, and non-invasive *in vivo* imaging [30]. In clinical practice, it is widely used in dermatology [31] and ophthalmology [32]. Due to the non-contact, non-invasive and high-resolution characters, OCT provides high-quality imaging for intraoperative tumor diagnosis [33]. Based on red blood cells, OCTA can realize blood anatomic information and functional information, such as vascular wall, tube diameter, angiogenesis [34]. OCTA has the advantages of simple operation and high spatial resolution [35]. The technology of OCTA provides new research ideas for monitoring tumor blood vessels.

In this study, we fabricated intelligent nano-sized polymersomes to achieve synergistic PTT/PDT-chemo-antiangiogenic therapy under the evaluation of OCTA/ NIRF dual-modal imaging (Scheme 1). Indocyanine green (ICG) was transferred to hydrophobic ICG-tetrabutylamine salt and incorporated within the hydrophobic membrane to act as contrast agent as well as photothermal conversion agent and photosensitizer. SOR, a molecular targeted drug with poor water solubility, was also encapsulated within the membrane of the polymersomes to possess both antiangiogenic and antitumor effects. Ammonium bicarbonate (ABC) and mitoxantrone (MIT) were loaded in the hydrophilic cavity of the polymersomes to realize stimuli-responsiveness and chemotherapy, respectively. The drugs-loaded polymersomes were modified with DSPE-PEG-Folate (denoted as FA-MIT-SIPS) to facilitate active tumor targeting and cellular uptake by folate receptors (FR)-mediated endocytosis. After intravenous injection, the FA-MIT-SIPS can effectively accumulate and penetrate in tumors *via* enhanced permeability and retention (EPR) and FA-targeting effect. In acid or hyperthermia condition, the decomposition of ABC would destroy the structure of FA-MIT-SIPS to accelerate drug release. The released MIT accumulated in nucleus to induce DNA damage, while the released SOR inhibited cell proliferation and destroyed tumor vascularization. Under laser irradiation, the ICG produced hyperthermia and ROS for effective PTT and PDT. Besides, its structure and concentration would change the optical scattering characteristic of OCTA system. To our knowledge, this is a novel work utilizing well-designed "all-in-one" polymersomes for tumor synergistic chemo/photo/antiangiogenic therapy under the guidance of OCTA/NIRF dual-modal imaging.

FA-MIT-SIPS were synthesized by thin-film hydration and concentration gradient diffusion method. The appearance of the formulated FA-MIT-SIPS was observed by AFM and exhibited uniform spherical shape with a diameter of ~200 nm (Fig. 1A). The particle size and zeta potential of various polymersomes were measured by a NanoZS Zetasizer (Figs. 1B and C). The average diameter of FA-MIT-SIPS was 206 ± 11.42 nm with polydispersity index (PDI) of 0.28 ± 0.05. The polymersomes displayed stable negative potential, which was beneficial to avoid them being quickly cleared by the body during circulation [36]. UV–vis spectrophotometer and HPLC were exploited to accurately quantify the drug content in the polymersomes. The EE and DL of MIT, ICG and SOR were exhibited in Table S1 (Supporting information). The cumulative MIT and SOR release from FA-MIT-SIPS in PBS with or without laser irradiation were detected by HPLC (Fig. S1 in Supporting information). In PBS at pH 5.5, FA-MIT-SIPS + laser completely released MIT at 168 h, while SOR only released 88.40% at the time.

The results showed that FA-MIT-SIPS were able to enhance the release of MIT and SOR in responsive to the acidic tumor environment and hyperthermia produced by ICG under laser irradiation. The temperature changes of FA-MIT-SIPS induced by 808 nm laser irradiation within 5 min were monitored and displayed in Figs. 1D and E. And it was found that PTT effect was dependent on laser power intensity and the concentration of FA-MIT-SIPS. In addition, the infrared photos of FA-MIT-SIPS and free ICG with an equivalent ICG concentration of 7.0 μg/mL under 1.5 W/cm^2 808 nm laser were obtained at T_{max} (Fig. 1F). The maximal temperature of FA-MIT-SIPS was 51.7 °C, which could kill tumor cells. However, the maximal temperature of free ICG was 43.0 °C, which may be caused by its instability in aqueous solution and proneness of photobleaching.

The cellular uptake of MIT and ICG in various formulations with or without laser irradiation was observed using CLSM (Fig. 2A). Free ICG was internalized less than the ICG in the polymersomes and trapped in the cytoplasm due to its binding with glutathione

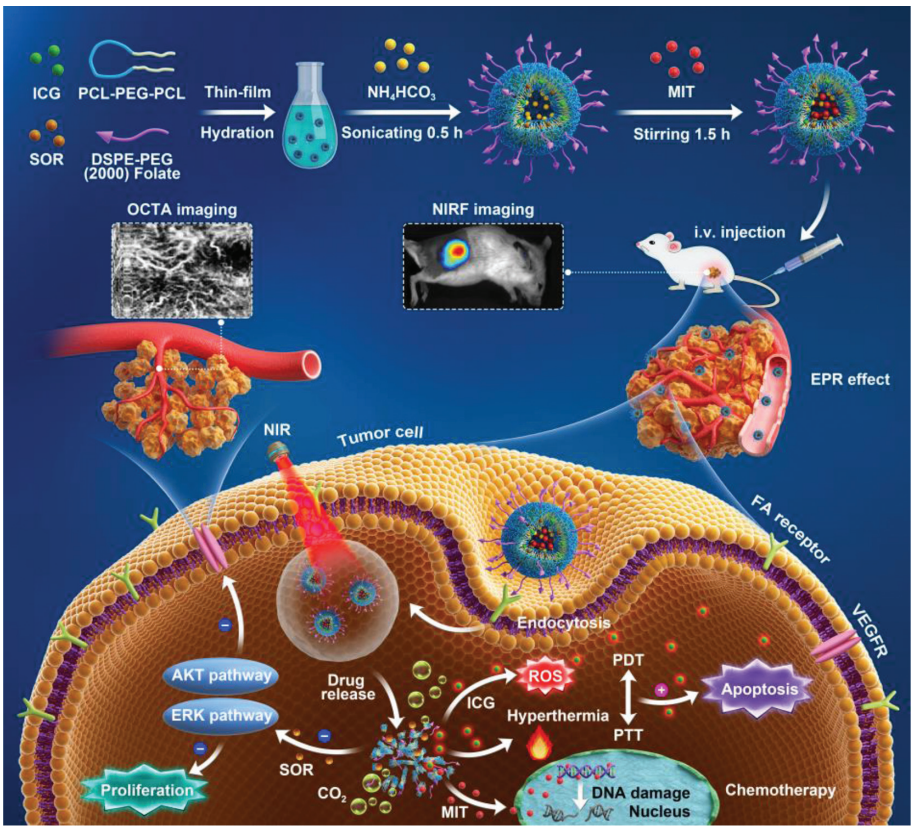

Scheme 1. Schematic illustration of the assembly of the intelligent drugs-loaded polymersomes (FA-MIT-SIPS) and the synergistic cancer photo-chemo-antiangiogenic therapy and *in vivo* evaluation *via* OCTA/NIRF dual-modal imaging.

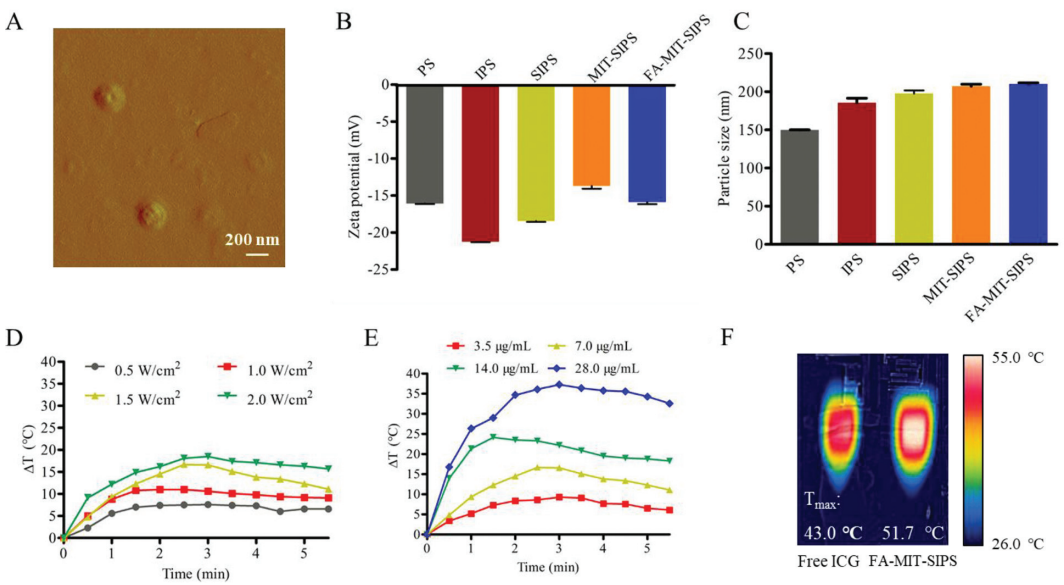

Fig. 1. Characterization of FA-MIT-SIPS. (A) Representative AFM image of FA-MIT-SIPS (scale bar: 200 nm). (B) Particle size and (C) zeta potential values of different polymersomes. (D) Photothermal effect of FA-MIT-SIPS at 7.0 μg/mL. (E) Photothermal effect of FA-MIT-SIPS under 808 nm laser irradiation (1.5 W/cm^2, 5 min). (F) Thermal images of free ICG and FA-MIT-SIPS with an equivalent ICG concentration of 7.0 μg/mL under 808 nm laser irradiation (1.5 W/cm^2, 5 min).

s-transferase protein, while free MIT was internalized more than the MIT in the polymersomes and transported to the nucleus to intercalate DNA [37]. The fluorescence signals of both MIT and ICG in the folate-modified group (FA-MIT-SIPS) were markedly stronger, demonstrating that folate modification enhanced cellular uptake in 4T1 cells with overexpression of folate receptor [38]. The internalization of MIT and ICG in all preparations was significantly increased when the cells were irradiated by 808 nm laser, which might be due to that the hyperthermia generated by PTT and ROS induced by PDT can enhance intracellular drug delivery and release *via* the increased fluidity of cell membranes and disruption of endosomes [39]. MTS assay was performed to detect the cytotoxicity of different formulations with various concentrations (Fig. S2 in Supporting information). With the increase of

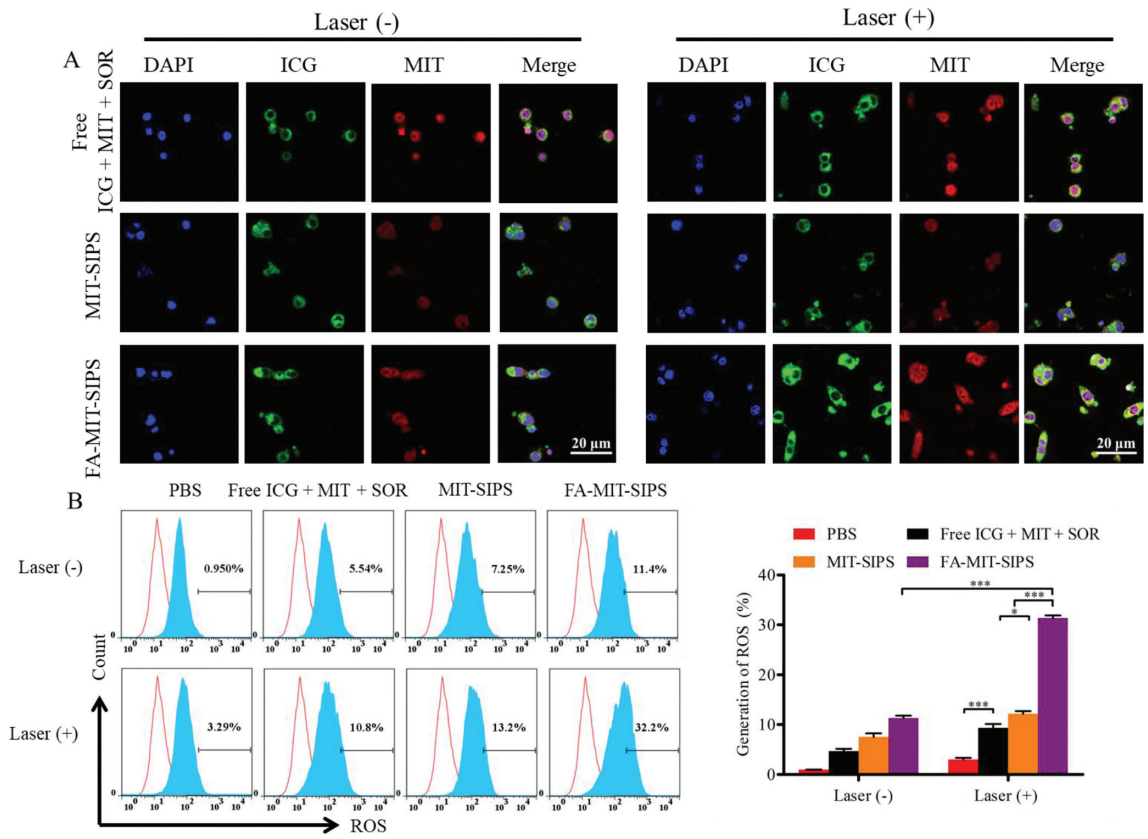

Fig. 2. (A) Effect of cellular uptake *in vitro*. CLSM images of cellular uptake in 4T1 cells after incubating with free ICG + MIT + SOR, MIT-SIPS or FA-MIT-SIPS for 12 h. (B) ROS generation in 4T1 cells incubated with various formulations (the red curve was the negative control group).

drug concentrations, the cell viabilities were gradually decreased after incubating with MIT or SOR-loaded polymersomes. FA-MIT-SIPS exhibited a superior cytotoxicity over MIT-SIPS, resulting from the FA-mediated higher cellular endocytosis. What is more, FA-MIT-SIPS + Laser displayed the strongest cytotoxicity among all the groups, demonstrating the synergistic effect of the three drugs. The cells treated with blank polymersomes had a good survival, indicating the safety and biocompatibility of the nanocarrier.

The generation of ROS in the cells and the quantitative analysis was performed by flow cytometry (Fig. 2B). The cells treated with various formulations without laser irradiation produced weak or negligible ROS. After receiving 808 nm laser irradiation, the cells in each group generated more ROS. The fluorescence intensity of MIT-SIPS + Laser group was 13.2%, which was dramatically higher than that of free ICG + MIT + SOR + Laser group (10.8%), owing to that the polymersomes enhanced the stability and intracellular delivery of ICG. FA-MIT-SIPS + Laser further increased the ROS fluorescence intensity to 32.2%, contributing to that FA conjugation promoted folate receptor-mediated cellular uptake.

CRI Maestro imaging system was used to obtain NIRF imaging to observe the *in vivo* bio-distribution of the polymersomes at predetermined time points (Fig. 3A and Fig. S3 in Supporting information). The ICG fluorescence intensity of all groups increased with time and reached a maximum at 24 h following the intravenous injection. At each time point, the ICG fluorescence intensity of the free ICG + MIT + SOR group was the lowest, which may be owing to the short plasma half-life and non-target specificity of free ICG. The polymersomes promoted the accumulation of ICG into the tumor. Notably, FA-modified polymersomes exhibited more accumulation compared to untargeted group. After intravenous injection for 24 h, the fluorescence signal decreased gradually. Meanwhile, the ICG fluorescence signal of FA-MIT-SIPS combined with laser dropped sharply at 48 and 72 h The results above demonstrated that FA-MIT-SIPS favored the accumulation and residence of drugs at the tumor site. The temperature change and thermal images were recorded by an IR thermal camera (Fig. 3B and Fig. S3). The free ICG + MIT + SOR group showed weak photothermal effect with the highest temperature of 42.2 °C under 808 nm laser irradiation. However, the highest temperature increased to 48.4 °C for the MIT-SIPS group, contributing to that the polymersomes promoted drug accumulation within tumors and enhanced photothermal conversion efficiency. Furthermore, the maximum temperature of FA-modified polymersomes was above 52 °C, which was high enough to effectively ablate tumor cells.

The microvascular blood flow changes in specific site of the tumor during chemo-phototherapy and tumor growth were studied using a self-made swept source OCTA system. As shown in Fig. S4A (Supporting information), the swept laser source was capable of a center wavelength of 1310 nm, a repetition frequency of 100 kHz, and a half-peak width of 140 nm. The interference light signal was converted into an electrical signal by a balanced detector (BPD), and then transmitted to the data acquisition device. The original data was processed by the image processing module to realize the display and storage of the images. In detail, the system can provide an approximately 5 mm × 5 mm field of view, with 256 A lines in each B scan (Fig. S4B in Supporting information). The C scan included 256 locations, and eight repetitive B scans were performed in the same location. The blood flow dynamics information was obtained through an improved speckle contrast optical coherence tomography algorithm (ISC-OCTA) [40]. 24 h after intravenous administration of various formulations in mice was recorded as day 0. The mice were anesthetized to capture images of tumor microvascular blood flow on days 0, 1, 2, 4, 6, and 10, respectively. En-face blood flow results were shown in Fig. 3C. Red blood cell (RBC)

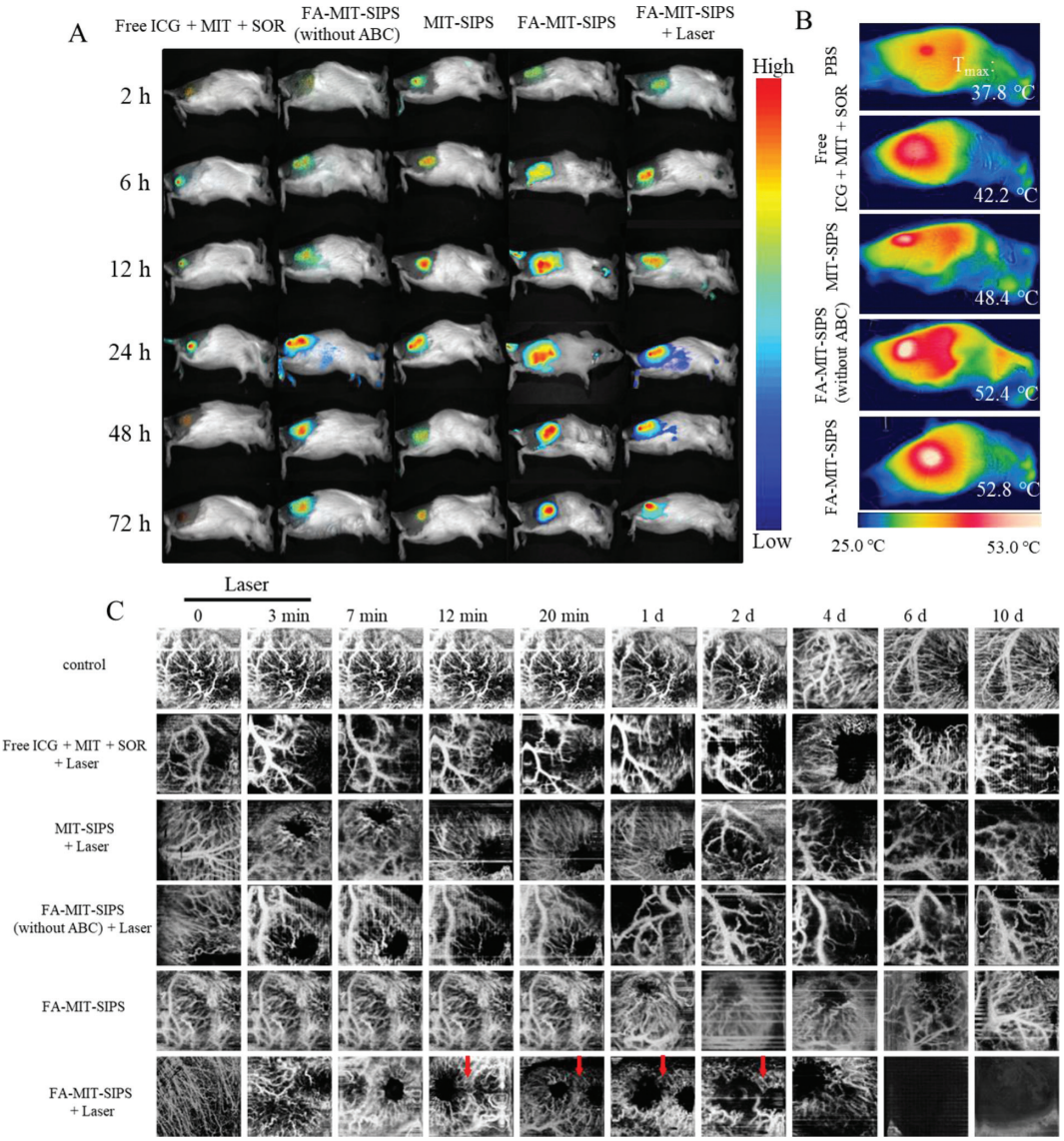

Fig. 3. Drug distribution and vascular imaging *in vivo*. (A) *In vivo* NIR fluorescence images after intravenous injection of free ICG + MIT + SOR, FA-MIT-SIPS (without ABC), MIT-SIPS, and FA-MIT-SIPS in 4T1 tumor-bearing mice at different time points ($n = 3$). (B) Thermal images of 4T1 tumor-bearing mice in different groups under 808 nm laser irradiation (1.5 W/cm^2, $n = 3$). (C) Representative OCTA images at different time points for each group. The red arrows represented the obvious changes at the same area ($n = 5$).

was regarded as contrast agents to extract blood flow functional information in the system of OCTA [26]. The autonomic movement of mice was common during the process of irradiation, so they were anesthetized. Vessel area density (VAD) is an important parameter to measure blood vessel function. For different formulations, the value of VAD based on OCT system was calculated during treatment. There was no difference in PBS group during the treatment (Fig. S5 in Supporting information). VAD decreased slowly after laser irradiation in free ICG + MIT + SOR group (Fig. S5). Especially, the microvascular blood flow returned to their normal state in free ICG + MIT + SOR group, indicating that it did not cause irreversible blood flow changes. The value of VAD was statistically different in the MIT-SIPS + Laser group compared with the initial value (Fig. S5). The microvascular blood flow disappeared at 2 d in the FA-MIT-SIPS (without ABC) group, but it reappeared at 6 d (Fig. S3). Tumors from tissue dissection were also found in the FA-MIT-SIPS (without ABC) group. There was a risk of tumor recurrence in FA-MIT-SIPS (without ABC). There was no difference in VAD in FA-MIT-SIPS group during treatment, and the drug system could not achieve antitumor effect only relied on pH response (Fig. S5). The microvascular blood flow network reduced after laser irradiation, VAD decreased obviously with time and reached a minimum at 6 d (Fig. S5). VAD increased slightly at 10 d in FA-MIT-SIPS + Laser group, the reason of which was blood flow returned to normal state from the skin. That was consistent with tissue dissection. Compared with MIT-SIPS + Laser group, VAD was decreased steadily in FA-MIT-SIPS + Laser group due to FA-targeting effect. Laser irradiation not only promoted the antitumor effect, but also affected the state of microvascular blood flow. All animals were treated according to the regulations and guidelines of the Institute of Biomedical Engineering, Chinese Academy of Medical Science & Peking Union Medical College.

The antitumor effect of FA-MIT-SIPS combined with 808 nm laser irradiation was evaluated in 4T1 tumor-bearing mice, and the experimental protocol was listed in Fig. 4A. ROS production, MIT accumulation and tumor cell apoptosis after treatment with vari-

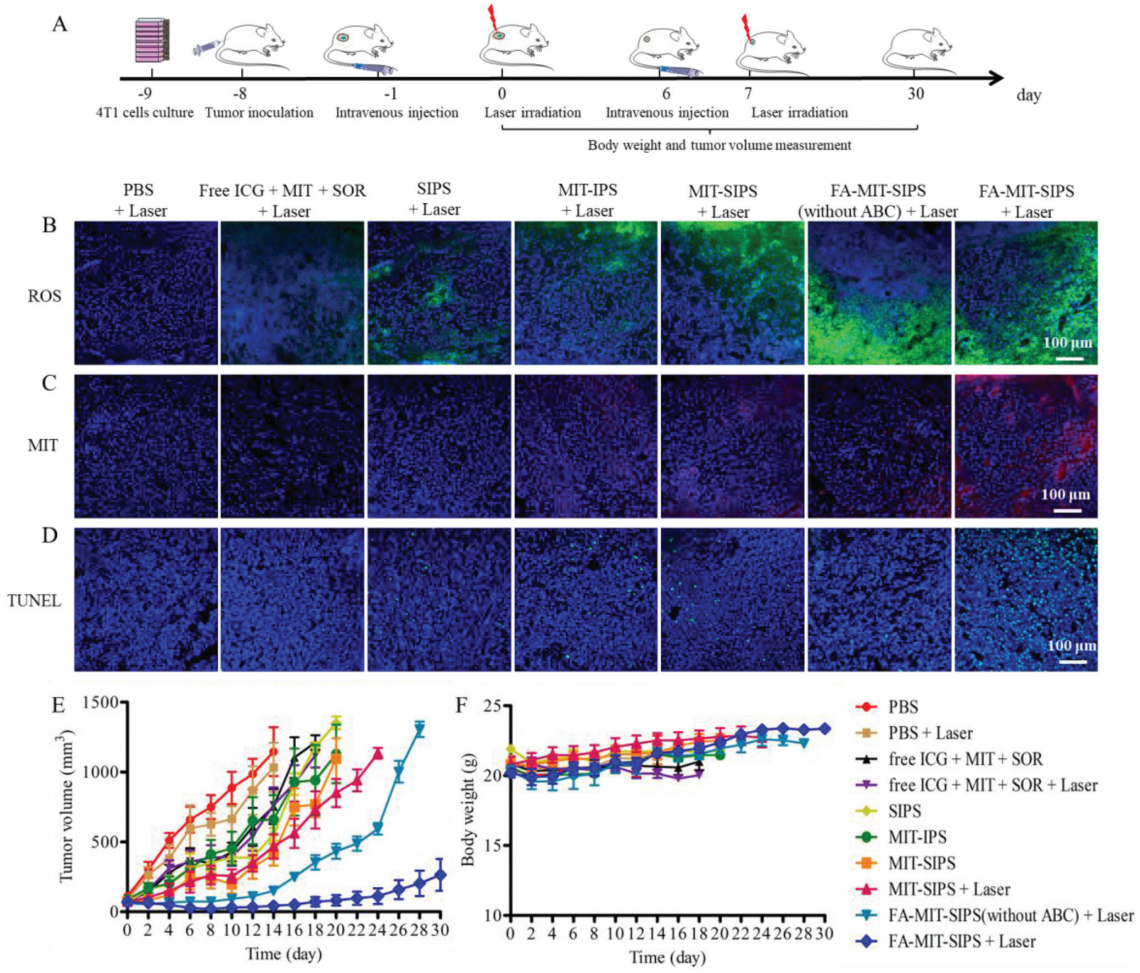

Fig. 4. *In vivo* antitumor effect evaluation. (A) Schematic diagram of the model establishment and treatment. CLSM images of tumor slices to observe (B) ROS production, (C) MIT accumulation, and (D) TUNEL assay (scale bar: 100 μm). (E) Tumor volume and (F) body weight curves of 4T1 tumor-bearing mice for each group ($n = 5$).

ous formulations were studied. Free ICG + MIT + SOR + Laser group only showed weak green fluorescence, whereas ICG-loaded polymersomes (SIPS + Laser, MIT-IPS + Laser, and MIT-SIPS + Laser) had notable green fluorescence, confirming that ROS production was increased due to the accumulation of ICG in the tumors *via* polymersomes delivery (Fig. 4B). Furthermore, FA-MIT-SIPS (without ABC) + Laser and FA-MIT-SIPS + Laser group displayed remarkably brighter green fluorescence, indicating that ROS was efficiently generated in the FA-targeting polymersomes after laser irradiation. Fig. 4C depicted that MIT accumulation was also significantly increased in the FA-MIT-SIPS + Laser group, showing much brighter red MIT fluorescence than the other groups. Compared with FA-MIT-SIPS (without ABC) group, FA-MIT-SIPS group exhibited a marked increase of red fluorescence. This might be due to that the ABC incorporation within the polymersomes accelerated intracellular MIT delivery and release in responsive to hyperthermia and low pH value. TUNEL assay was carried out to evaluate the apoptosis in the tumor tissues after various treatments. As shown in Fig. 4D, a more significantly higher apoptosis was observed for the FA-MIT-SIPS + Laser group, confirming the synergistic effect of targeted co-delivery polymersomes on eradicating tumor cells.

To further prove the combination anticancer capability of FA-MIT-SIPS under laser irradiation, the volume changes of the tumors were observed for one month. As shown in Fig. 4E, the tumor volumes in PBS and PBS + Laser group increased very rapidly, indicating that laser irradiation alone almost had no effect on inhibiting tumor growth. For the mice injected with free ICG + MIT + SOR, the tumor growth was slightly delayed, due to the rapid clearance and low accumulation of free drugs in tumor tissues. Compared with SIPS, MIT-IPS, or MIT-SIPS group, MIT-SIPS + Laser group exhibited slightly more tumor inhibition, probably contributing to the synergistic effect under laser treatment. Inspiringly, FA-MIT-SIPS + Laser exhibited the highest antitumor efficacy among all the groups and 2 out of 5 mice were completely cured without recurrence during the monitoring period (30 days post the first laser irradiation). The excellent antitumor ability of FA-MIT-SIPS combined with laser irradiation assuredly ascribed to that the formulated FA-targeting polymersomes efficiently accumulated in tumor sites, realized intracellular drug delivery and stimuli-responsive release, and achieved synergistic PTT/PDT-chemo-antiangiogenic therapy. As shown in Fig. 4F, no severe body weight loss was observed for the mice in all the groups, indicating that the mice were well tolerated during the experimental period.

Since SOR is a multi-kinase inhibitor that can inhibit VEGF and PDGF receptors, its effect on tumor angiogenesis was observed by CD31 immunohistochemistry staining (Fig. S6 in Supporting information). CD31 positive area was the lowest in the FA-MIT-SIPS + Laser group, demonstrating great inhibition on tumor angiogenesis for the mice treated by FA-targeting co-delivery polymersomes under laser irradiation, which would further lead to tumor cell apoptosis. In addition, H&E staining was applied to verify the anticancer effect of various groups (Fig. S6). MIT-SIPS + Laser and FA-MIT-SIPS (without ABC) + Laser group had obvious tumor necrosis. Importantly, the tumor tissues in the mice treated by FA-

MIT-SIPS + Laser group exhibited severe necrosis with greatly decreased cell numbers, indicating that FA-MIT-SIPS in combination with laser irradiation significantly eradicated cancer cells. Finally, in order to verify the biological safety, the main organs of the mice were collected and stained by H&E on day 6 (Fig. S7 in Supporting information). It showed that there was no obvious tissue damage for FA-MIT-SIPS + Laser treated group, indicating that FA-MIT-SIPS exhibited good biocompatibility and safety. Besides, it was worth mentioning that free MIT exhibited cardiotoxicity.

In summary, we reported folate-targeted co-delivery polymersomes for tumor synergistic photo-chemo-antiangiogenic therapy and *in vivo* evaluation *via* OCTA/NIRF dual-modal imaging. The fabricated intelligent polymersomes co-delivered both hydrophobic and hydrophilic therapeutics (denoted as FA-MIT-SIPS), enhanced cellular uptake, and facilitated drug release under acidic condition and laser irradiation, showing excellent *in vitro* antitumor activity. More importantly, OCTA/NIRF dual-modal imaging has been applied in the process of antitumor effect evaluation. Dual-modal imaging showed that the FA-MIT-SIPS could not only enrich in the tumor, but also provide the blood flow information during the treatment. Significantly, FA-MIT-SIPS achieved remarkable *in vivo* antitumor effect under the synergistic PTT/PDT-chemo-antiangiogenic therapy. Hence, FA-MIT-SIPS is a promising "all-in-one" nanoplatform for cancer diagnosis and treatment with excellent efficacy and biosafety.

Declaration of competing interest

The authors declare that they have no known competing financial interests or personal relationships that could have appeared to influence the work reported in this paper.

Acknowledgments

This work was financially supported by the National Natural Science Foundation of China (Nos. 82072059 and 82172090), the Fundamental Research Funds for the Central Universities (No. 2019PT320028), Tianjin Municipal Natural Science Foundation (No. 20JCYBJC00030), CAMS Initiative for Innovative Medicine (No. 2021-I2M-1–058) and Science and Technology Planning Project of Tianjin (No. 18ZXSGSY00050).

Supplementary materials

Supplementary material associated with this article can be found, in the online version, at doi:10.1016/j.cclet.2022.04.021.

References

[1] H. Zhao, C. Liu, Z. Gu, et al., Nano Lett. 20 (2020) 252–260.
[2] J. Zhang, C. Li, Q. Xue, et al., Small Methods 5 (2021) e2100539.
[3] R. Nussinov, C. Tsai, H. Jang, Drug Resist. Updates 12 (2021) 100796.
[4] S. Lal, S.E. Clare, N.J. Halas, Acc. Chem. Res. 41 (2008) 1842–1851.
[5] Z. Li, F. Fan, J. Ma, et al., Biomater. Sci. 9 (2021) 5841–5853.
[6] W. Ni, J. Wu, H. Fang, et al., Nano Lett. 21 (2021) 7796–7805.
[7] L. Chen, X. Meng, M. Liu, et al., ACS Appl. Mater. Interfaces 12 (2020) 30234–30246v.
[8] H. Yi, W. Lu, F. Liu, et al., J. Nanobiotechnol. 19 (2021) 134.
[9] K. Nones, J. Johnson, F. Newell, et al., Annal. Oncol. 30 (2019) 1071–1079.
[10] S. Sharma, A.P. Mann, T. Lder, et al., J. Control. Release 268 (2017) 49–56.
[11] C. Viallard, B. Larrivée, Angiogenesis 20 (2017) 409–426.
[12] Q. Li, R. Zhou, Y. Sun, et al., ACS Appl. Mater. Interfaces 13 (2021) 11708–11720.
[13] R. Gao, R. Kalathur, M. Coto-Llerena, et al., EMBO Mol. Med. 12 (2021) e14351.
[14] S.M. Weis, D.A. Cheresh, Nat. Med. 17 (2011) 1359–1370.
[15] J. Sui, Y. Cui, H. Cai, et al., Nanoscale 9 (2017) 2755–2767.
[16] F. Chen, Y. Fang, X. Chen, et al., Asian J. Pharmaceut. Sci. 16 (2020) 318–336.
[17] F. Chen, Y. Fang, R. Zhao, et al., Eur. J. Med. Chem. 179 (2019) 916–935.
[18] R. Maharjan, J. Choi, S. Kweon, et al., Biomaterials 281 (2021) 121334.
[19] H. Zhang, J. Bussmann, F. Huhnke, et al., Adv. Sci. 12 (2021) e2102072.
[20] B. Maya, B. Iak, D. Yhaec, et al., J. Control. Release 331 (2021) 335–349.
[21] A.K. Sharma, P. Prasher, A.A. Aljabali, et al., Drug Deliv. Transl. Res. 10 (2020) 1171–1190.
[22] J. Leong, J. Teo, V. Aakalu, et al., Adv. Healthc. Mater. 7 (2018) e1701276.
[23] T. Sun, A. Dasgupta, Z. Zhao, et al., Adv. Drug Deliv. Rev. 158 (2020) 36–62.
[24] C. Pérez-Medina, A. Teunissen, E. Kluza, et al., Adv. Drug Deliv. Rev. 11 (2020) 154–155.
[25] R. Yang, K. Lou, P. Wang, et al., Small Methods 5 (2021) 2001066.
[26] A. Kashani, C. Chen, J. Gahm, et al., Progr. Retinal Eye Res. 60 (2017) 66–100.
[27] Y. Zhu, F. Zhu, Z. Ding, et al., J. Biophoton. 14 (2021) 202000370.
[28] W. Wu, B. Khan, M. Sharzehee, et al., Sci. Rep. 11 (2021) 12252.
[29] R.K. Wang, A. Lin, S. Saunders, D.J. Wilson, Biomed. Opt. 15 (2010) 020502.
[30] W. Yuan, D. Chen, R. Sarabia-Estrada, et al., Sci. Adv. 6 (2020) 9664.
[31] B. Wan, C. Ganier, X. Du-Harpur, et al., Br. J. Dermatol. 184 (2021) 1014–1022.
[32] V. Nguyen, W. Fan, T. Zhu, et al., ACS Nano 15 (2021) 13289–13306.
[33] D. Zhu, J. Wang, M. Marjanovic, et al., Biomed. Opt. Express 12 (2021) 3021–3036.
[34] D. Huang, G. Wang, J. Mao, et al., Adv. Sci. 8 (2021) 2101242.
[35] M. Fujino, F. Otsuka, T. Noguchi, S. Yasuda, Eur. Heart J. 41 (2020) 4446.
[36] C. Guo, L. Sun, H. Cai, et al., ACS Appl. Mater. Interfaces 9 (2017) 23508–23519.
[37] Z. Chen, P. Zhao, Z. Luo, et al., ACS Nano 10 (2016) 10049–10057.
[38] Zhou Chen, Lulu, et al., Adv. Mater. 31 (2019) 1336–1345.
[39] W. Fan, B. Yung, P. Huang, X. Chen, Chem. Rev. 117 (2017) 13566–13638.
[40] L. Wang, Y. Li, Y. Li, K. Li, Am. J. Transl. Res. 10 (2018) 3025–3035.